A Time-Delay Equivalent-Circuit Model of Ultrafast p-i-n Photodiodes

Gang Wang, Tsuneo Tokumitsu, *Senior Member, IEEE*, Ikuo Hanawa, Yoshihiro Yoneda, Keiji Sato, and Masahiro Kobayashi

***Abstract*—A time-delay equivalent-circuit model of ultrafast p-i-n photodiodes (PDs) is proposed to describe the operation at high-input power levels. This model includes both the carrier transit-induced time-delay effect and stored charge effect of p-i-n PDs in high-power operation. These effects were represented as a linear RC circuit [1] and capacitance, respectively, both combined in parallel to a voltage-controlled current source. The validity of this model was confirmed with good curve fitting to the measured optical-frequency responses of an ultrafast side-illuminated p-i-n PD.**

***Index Terms*—Equivalent circuit, optical-frequency response, photodiodes (PDs), scattering parameters, stored charge, time delay.**

I. Introduction

PHOTO receivers plays an important role in the optical-fiber system, and the operating frequency range has been expanded to the millimeter-wave region. Since optical-fiber amplifiers have been recently used in high-speed optical transmission systems at 40 Gb/s and beyond, the ultrafast photodiodes (PDs) used in the photo receivers are currently required to operate for a high-power illumination [2]. Much research has been done to numerically and experimentally investigate the high-power performance of PDs [3]. It is suggested that the modulation bandwidth and eye diagrams of photo receivers at high bit rates can be degraded due to the increased space charge effects suffered from the carriers generated by illumination when they transit through the depletion region of the PDs under high-power illumination. On the other hand, the use of a computer-aided equivalent-circuit simulation system becomes very important in the design of high-performance photo receivers since the final performance of the photo receivers must be confirmed in advance before they are fabricated. It is usually convenient to apply a physic-based equivalent-circuit models of PDs in such a circuit simulator, however, very few reported equivalent-circuit model treated the transit time effect by fully electrical equivalent-circuit models [4]–[6].

In our previous research, we proposed a small-signal electrical-circuit model that includes a carrier transit-induced time delay represented with an RC time constant [1]. This linear RC circuit, which is combined in parallel to a voltage-controlled current source (VCCS), represented well the high-frequency response of our side-illuminated p-i-n PDs when the optical input power level was set to be less than 10 mW for linear operation. However, it is found that it is difficult to use the previously proposed linear RC circuit model to represent the nonlinear frequency responses, which is observed in the studied p-i-n PDs beyond 10 mW, because of a lack of some physical effect. In this paper, we propose a fully electrical time-delay equivalent-circuit model to represent the high-power high-frequency response of p-i-n PDs. This model equivalently represents the high-power illumination-induced stored charge effect in the p-i-n PDs because of a newly added capacitance $C_{\rm sc}$ element in parallel to the linear RC circuit elements R_t and C_t. All of the above three time-delay circuit elements R_t, C_t, and $C_{\rm sc}$ were treated as voltage-dependent components, and each behavior was measured based on the best curve fitting using the new equivalent-circuit model. This analysis made the PDs' high-power nonlinear behavior clearly visible, as well as having proved the effectiveness of the new equivalent-circuit model.

Manuscript received July 7, 2002; revised October 28, 2002.

The authors are with Fujitsu Quantum Devices Limited, Yamanashi 409-3883, Japan.

Digital Object Identifier 10.1109/TMTT.2003.809642

II. Experimental Procedures

As shown in Fig. 1(a), a side-illuminated p^+-InP/i–InGaAs/n-InP waveguide-integrated double-heterojunction p-i-n photodiodes (WG p-i-n PDs) is used for optical frequency response analysis and equivalent-circuit model design. The waveguide of this PDs functions as a spot-size converter in which the thickness of an InGaAsP core tapers in the propagation direction. The waveguide was fabricated by using selective MOCVD growth technology. The p-i-n junction area is 6 μm$\times$ 7μm and the thickness of the InGaAs optical absorption layer is 0.28 μm. The p-i-n junction area is buried in semi-insulating InP. To reduce the parasitic capacitance, the bonding pad of the p-electrode was fabricated on the semi-insulating InP substrate, and the p-i-n junction area and the bonding pad are connected by an air-bridge wire. The details of the device structure are described in [7]. Fig. 1(b) indicates how the parasitic components are connected and related to the physical parameters of the WG p-i-n PDs, where R_c is the p-electrode contact resistance, R_j is the resistance of the P^+-InP layer; C_j is the reverse-bias junction capacitance, C_{dx} is the capacitance between the air bridge and n-electrode pad, C_p is the p-electrode pad capacitance, L_s is the inductance of the air-bridge from p-contact to p-electrode pad, and L_G is the inductance induced by the n-electrode pad as an RF ground pattern.

Frequency-domain optical responses (S_{21}) and the reflection coefficients (S_{22}) of the studied WG p-i-n PD were measured by using 50-GHz lightwave component analyzer equipment

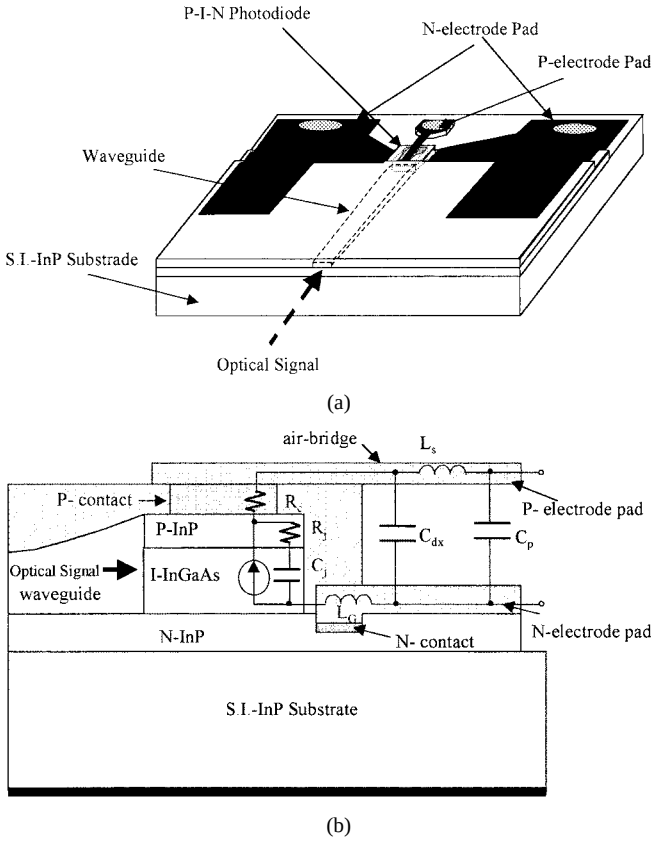

Fig. 1. (a) Schematic structure. (b) Cross section of a side-illuminated waveguide-integrated p-i-n PD. The equivalent-circuit elements are related to the p-i-n PD parameters as shown.

(HP/Agilent 8603A). The laser with a 1550-nm center wavelength was used as the measurement source. The device was contacted by a 50-Ω ground–signal–ground (GSG) microwave probe. The measured 3-dB bandwidth $f_{3\text{-dB}}$ for the sample is over 35 GHz at -5-V bias voltage and below 10-mW optical input power.

III. Time-Delay Small-Signal Equivalent Circuits of p-i-n PDs

Fig. 2 shows the small-signal equivalent circuit [1] that considers both the carrier transit-induced time delay and the parasitic elements for the studied WG p-i-n PD. The carrier transit-induced time delay is equivalently represented by a linear RC circuit (Part I in Fig. 2, indicated as R_tC_t) combined with a VCCS. The basic design concept of this time-delay equivalent circuit is as follows.

1) The 3-dB electrical bandwidth of PD $(f_{3\,\text{dB}})$ is limited by both the carrier transit time and parasitic CR-time constant. Since these limiting factors are assumed to be independent of each other and have Gaussian responses [8], the $f_{3\,\text{dB}}$ of the PDs can be approximated as [9]

$$\frac{1}{f_{3\,\text{dB}}^2} = \frac{1}{f_t^2} + \frac{1}{f_{CR}^2} \tag{1}$$

where f_t is the 3-dB electrical bandwidth limited by the carrier transit time and f_{CR} is the 3-dB electrical bandwidth limited by the parasitic CR-time constant. Therefore, we can reasonably model these two limiting factors separately, and then combine the two modeled equivalent circuit with the proper method to give a final equivalent-circuit description of the PDs.

2) The carrier transit time that limits the 3-dB electrical bandwidth f_t is related to the phase delay created by the transition of carriers generated by illumination in the depletion region of p-i-n PDs. The carriers generated by illumination move with saturation velocity over the drift region due to the high electric field in the depletion region and suffer a time delay. These carriers can be equivalent to cathode-emitting free carriers, which induces a photo current. We assume that the input optical ac signal has a frequency ω and is approximated as an ac voltage signal of the form $e_i(\omega)$ superposed to the dc bias. The ac photo current $i(\omega)$ due to the ac signal is assumed to be uniform in space and consists of both the particle current and displacement current. Following an analysis given by Wang [10] for a reverse-biased p-i-n IMPATT avalanche diode, $i(\omega)$ is given by

$$i(\omega) = i\omega\varepsilon E(\omega) + \gamma i(\omega)\exp\left(\frac{-i\omega x}{v_s}\right). \tag{2}$$

The fist part in (1) is the displacement current, where $E(\omega)$ is the ac component of the field in the drift region, γ is the ratio of the ac conduction current to the total ac current, and v_s is the constant saturation drift velocity of the carrier in the drift region, respectively. For the p-i-n PD, v_s represents the saturation drift velocity of the carrier generated in the depletion region due to contributions of both hole and electron, while it depends on optical input power level. By solving $E(\omega)$ in (2) and integrating it over the drift region, the ac voltage $e_i(\omega)$ across the transit region and the resulted ac photo current $i(\omega)$ are related to each other with an impedance Z_d

$$Z_d = R + iX = \frac{e_i(\omega)}{i(\omega)}. \tag{3}$$

Moreover, when the WG p-i-n PD is used for high-power and high-speed operation, there will be some nonuniform charge distribution that results in nonuniformity on the electric field and transit velocity. The IMPATT (3) gives only a first-order approximation. However, the basic concept of using a linear circuit with an impedance Z_d, which will function as a delay block applied to the ac optical signal $e_i(\omega)$ (i.e., a block having as the input an optical power and as the output a delayed ac optical power, which is related to the time-delayed voltage $e_o(\omega)$) to equivalently represent the carrier-transit time-induced time delay well explained the high-frequency response of the studied WG p-i-n PD for relatively small power operation [1]. In our proposed time-delay equivalent circuit, as shown in Fig. 2, the impedance Z_d is represented by a linear R_tC_t circuit, and the 3-dB electrical bandwidth f_t limited by the carrier transit time can be equivalently expressed by the CR time constant of this proposed R_tC_t circuit. This is the

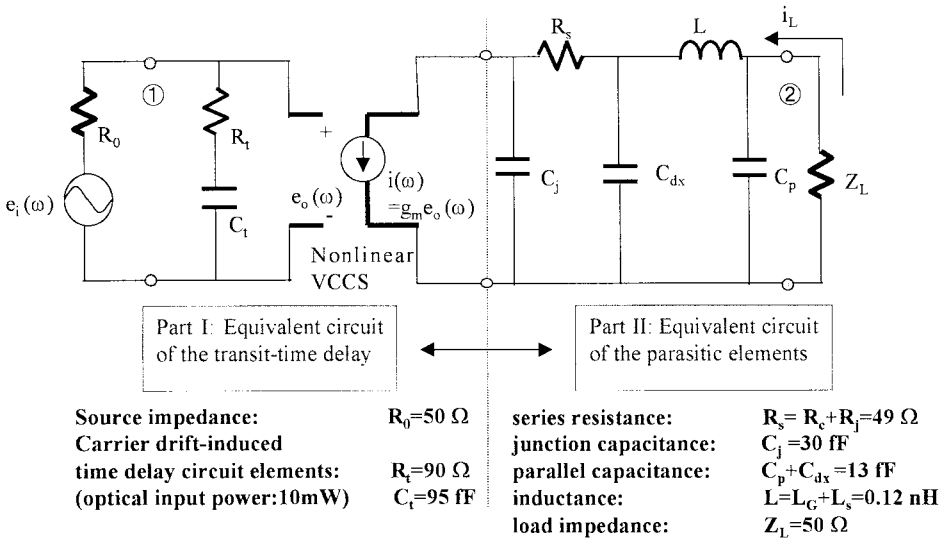

Fig. 2. Small-signal equivalent-circuit model of the side-illuminated WG p-i-n PD involving both the parasitic elements and carrier drift-induced time-delay effect.

physical-based consideration of Part I of the small-signal equivalent circuit shown in Fig. 2.

3) Now the time-delayed voltage $e_o(\omega)$ is assumed to create an ac photo current $i(\omega)$ flowing to the external parasitic circuits. Just like the discussion for FET, in the small-signal case and considering the first-order element of the RF signal, the ac element can be separately represented with the dc transconductance, and the relationship between $e_o(\omega)$ and $i(\omega)$ can be expressed as

$$i(\omega) = \frac{dI_{\rm dc}}{dV_{\rm dc}} e_o(\omega) = g_m e_o(\omega). \tag{4}$$

4) Since the WG p-i-n PD is electrically a lumped-element device, a set of parasitics due to the device structure is another bandwidth-limiting factor. The lumped parasitic circuit elements of the studied WG p-i-n PD shown in Fig. 1(b) is rearranged and shown as Part II in Fig. 2.

5) The ac photocurrent $i(\omega)$ that flows out to the external circuit is controlled by the delayed voltage $e_o(\omega)$ across the R_tC_t circuit. The VCCS is represented as $i(\omega) = g_m(e_o) \cdot e_o(\omega)$, where $g_m(e_o) \cdot e_o(0)$ gives the dc level and is considered equivalent to the optical conversion quantum efficiency.

As shown in Fig. 3(a) and (b), by carefully choosing the values for the circuit components shown in Fig. 2, the calculated optical frequency responses can be best fitted with the measured optical frequency responses of the studied WG p-i-n PD at a low-power-level small-signal operation, where the photocurrent is below 8.3 mA, which corresponds to an optical input power level of 10 mW. This procedure can be summarized as follow.

First, extraction of the parasitic values in the small-signal equivalent circuit were carried out by evaluating the S_{22}-parameter in the frequency range from 45 MHz to 50 GHz, as measured by the 50-GHz lightwave component analyzer. The extracted values for the WG p-i-n PD at -5-V bias voltage are also given in Fig. 2 (Part II). The best fitting exhibited a close agreement between the measured and calculated values, where

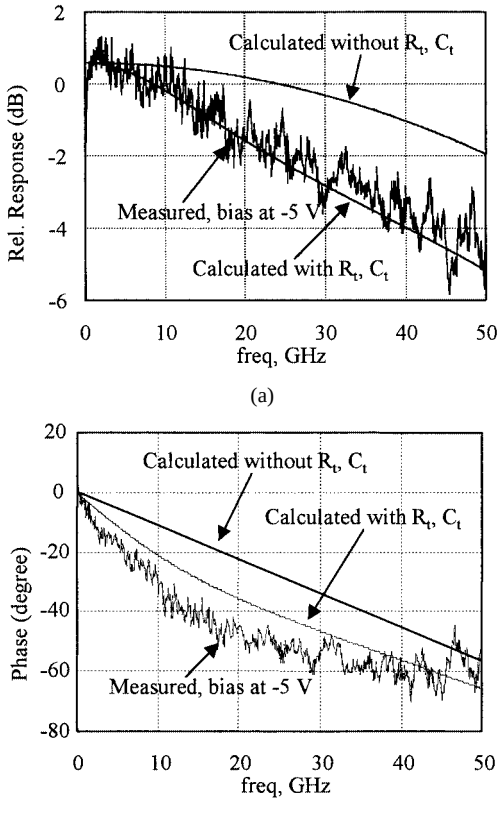

Fig. 3. Curve fitting of the: (a) magnitude and (b) phase shift of the small-signal response of the side-illuminated WG p-i-n PD. The calculated frequency response with and without circuit elements C_t and R_t are shown as solid lines.

the maximum fitting error levels in magnitude and phase difference of S_{22} are below 0.02% and $\pm 5^\circ$, respectively. In addition, the value of the total series resistances and total shunt capacitance are kept close to those for dc measurement at -5 V during the S_{22} curve-fitting procedure.

By carefully choosing the values for the carrier transit-induced time delay components (C_t, R_t, and g_m in Fig. 2), the

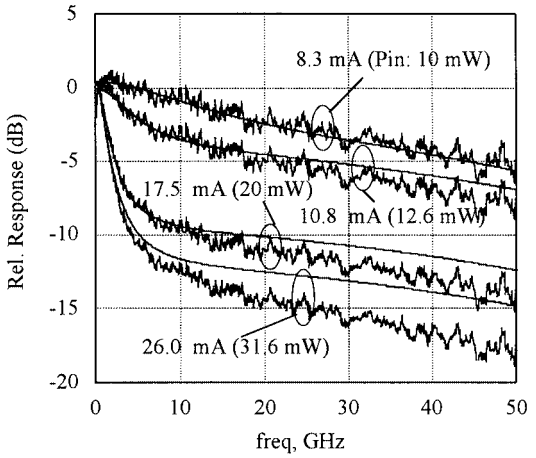

Fig. 4. Measured (noisy solid lines) and calculated (solid lines) optical frequency responses of the side-illuminated WG p-i-n PD at various input optical power levels. The experimental results are normalized to their low-frequency RF power levels, respectively.

calculated optical-frequency response can then be best fitted with the measured optical frequency response of the studied WG p-i-n PD. The calculated 3-dB bandwidth $f_{3\text{-dB}}$ of 35 GHz for this sample agrees well with the measured one. The maximum fitting error levels in magnitude and phase difference between measured and calculated S_{21} can be below 0.15% and $\pm 15^{\circ}$, respectively.

Finally, we adjusted the value of $g_m e_o(0)$ to make the dc level of the calculated optical response curve consistent with the measured one.

The noised solid lines in Fig. 4 show optical frequency responses of the studied WG p-i-n PD biased at -5 V at various photocurrent levels. The measured responses are compared to frequency responses calculated from the linear equivalent circuit in Fig. 2. The plots in this figure were normalized to their dc levels, respectively. The studied WG p-i-n PDs' response at an input optical power level of up to 10 mW (corresponds to a photocurrent value of 8.3 mA) can be reasonably curve fitted for constant C_t, R_t, and g_m. However, when increasing the photocurrent above 8.3 mA, the experimental frequency responses show a sudden collapse and a rapid drop at lower frequency. Hence, in the best curve fitting for the higher current levels, the values of transit-induced time-delay elements (C_t, R_t, and g_m in Fig. 2) were flexibly chosen for each lower frequency collapse response. The parasitic elements used in this calculation were not changed. The calculated frequency responses are shown in Fig. 4 with solid curves. It can be seen that even increasing the photocurrent above the critical current value (8.3 mA for the studied WG p-i-n PD), the calculated frequency responses still give a good agreement with the experimental collapse responses in the lower frequency range. On the other hand, it can also be seen that the equivalent circuit in Fig. 2 becomes not sufficient to produce a good fit with the high-frequency responses in the higher optical input power level condition, even though the carrier transit-induced time-delay components are variable.

In order to more exactly evaluate the optical frequency response of p-i-n PDs in a high current operating condition, a refinement to the small-signal equivalent-circuit model (as shown in Fig. 2) was performed by newly adding a parallel capacitance C_{sc} to the transit-induced time-delay equivalent-circuit elements C_t and R_t. Fig. 5 shows the newly proposed equivalent-circuit model, where the parasitic elements are the same with those shown in Fig. 2, Part II. As shown in Fig. 5, the delayed voltages over transit-induced time-delay equivalent-circuit element C_t and R_t and parallel capacitance C_{sc} are represented with $e_1(\omega)$ and $e_2(\omega)$, respectively. Now the overall delayed voltage $e_o(\omega)$ involves both the effects of $e_1(\omega)$ and $e_2(\omega)$. Otherwise, it can be seen the delayed voltage $e_o(\omega)$ of the time-delay element of the equivalent circuit shown in Fig. 2, Part I only involves the effect of $e_1(\omega)$. In view of the electrical circuit in Fig. 5, we can see that the time-delay circuit element C_t and R_t and the parallel capacitance C_{sc} provide two different types of delay block circuits with signal source impedance R_0, respectively. By identifying the optical power with the voltage generator $e_i(\omega)$, the relative optical-frequency responses of these two delay block circuits can be calculated as follows:

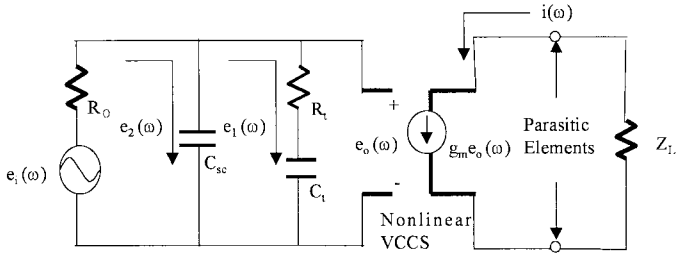

Fig. 5. High-power equivalent-circuit model of the side-illuminated WG p-i-n PD. The parasitic elements are the same as those shown in Fig. 2, Part II.

$$20\log\left|\frac{e_1(\omega)}{e_i(\omega)}\right| \text{ dB} = 20\log\left(\sqrt{\frac{1+\omega^2 C_t^2 R_t^2}{1+\{\omega C_t (R_0+R_t)\}^2}}\right) \text{ dB} \tag{5}$$

$$20\log\left|\frac{e_2(\omega)}{e_i(\omega)}\right| \text{ dB} = 20\log\left(\frac{1}{\sqrt{1+\omega^2 C_{\text{sc}}^2 R_0^2}}\right) \text{ dB}. \tag{6}$$

The calculated results are shown in Fig. 6. The values of the circuit elements used in the calculation are $R_t = 15\ \Omega$, $C_t = 2300$ fF, and $C_{\text{sc}} = 300$ fF, respectively. (As will be shown in Section IV, the values of R_t, C_t, and C_{sc} are the ones used to best curve fit the measured optical response of the studied WG p-i-n PD at a very high optical input level beyond 30 mW for the equivalent circuit in Fig. 5). The overall relative frequency response $e_0(\omega)$ (: $20\log|e_o(\omega)/e_i(\omega)|$) of the time-delay elements is dominated by a response of $e_1(\omega)$ (: $20\log|e_1(\omega)/e_i(\omega)|$) due to $R_t C_t$ in this high-power condition. However, as shown in Fig. 6, the overall optical-frequency response $20\log|e_o(\omega)/e_i(\omega)|$ shows an extra degradation in the higher frequency region compared with $20\log|e_1(\omega)/e_i(\omega)|$. It is clear that this effect is provided by the newly combined parallel capacitance C_{sc}. This extra response is performed before the RF signal is transferred to the external parasitic circuit. Hence, we think that the component C_{sc} seem to be a device physics-based parameter. The physical meaning of C_{sc} will be discussed in Section V.

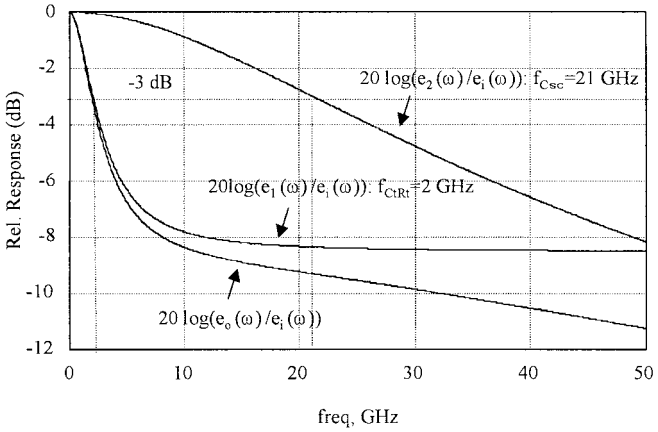

Fig. 6. Calculated frequency response of the newly proposed equivalent circuit shown in Fig. 5. $f_{C_t R_t}$ and $f_{C_{\rm sc}}$ represent the 3-dB electrical bandwidth of the linear $C_t R_t$ circuit and $C_{\rm sc}$ circuit, respectively.

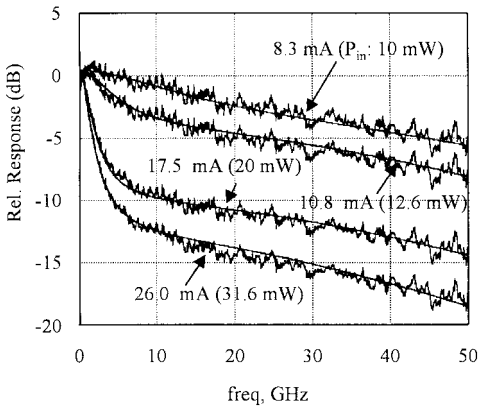

Fig. 7. Measured (noisy solid lines) and calculated (solid lines) optical frequency responses of the side-illuminated WG p-i-n PD for various input optical power levels. The experimental results are normalized to their low-frequency RF power levels, respectively.

IV. Curve-Fitting Results for High-Power Frequency Responses

To demonstrate the validity of our newly proposed equivalent-circuit model for a high-power operating condition, we have simulated the frequency response at high photocurrent conditions again using the same parasitic elements shown in Fig. 2. The simulation process is as follows: first, as described in Section III, the time-delay equivalent-circuit elements C_t, R_t, and g_m were chosen so that the calculated frequency response can be best fitted with the measured low-frequency optical response both in magnitude and phase. The parallel circuit element $C_{\rm sc}$ was then determined to make the calculated frequency response in the high-frequency region well fitted with the measured response both in magnitude and phase. The simulated frequency responses are depicted in Fig. 7 by solid lines. It can be seen that the simulated frequency responses using the proposed high-power equivalent circuit approximates very reasonably the measured optical-frequency responses of

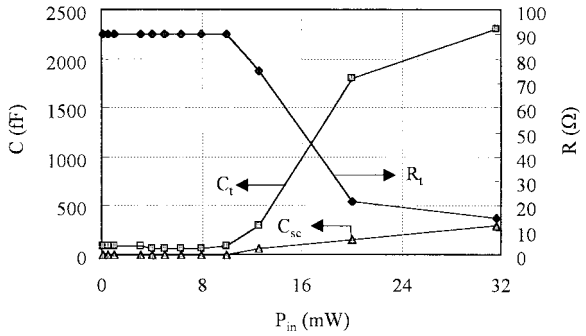

Fig. 8. Best-fitted values of the circuit elements C_t, R_t, and $C_{\rm sc}$ of the small-signal equivalent circuit as a function of optical input power levels.

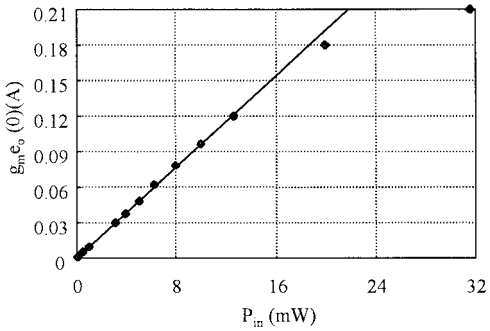

Fig. 9. Best-fitted values of dc response $g_m e_o(0)$ of the small-signal equivalent circuit as a function of optical input power levels.

the devices at various optical power (photocurrent) levels and in a broad frequency range from 45 MHz to 50 GHz.

The important issue in this curve fitting is that the physic-based parameters (C_t, R_t, g_m, and $C_{\rm sc}$) were treated as variables for input power levels. Figs. 8 and 9 shows the behavior of each variable for various optical input power ($P_{\rm in}$) levels. From Figs. 8 and 9, some important properties can be found as follows.

1) At an optical input power level (p-i-n) of below 10 mW (photocurrent: 8.3 mA), the measured optical-frequency response can be well fitted by only one set of time-delay circuit elements C_t, R_t, and g_m, where $C_{\rm sc} = 0$.
2) At an optical input power level of beyond 10 mW, the measured optical frequency response across the whole frequency region can be well represented by best choosing the value of the parallel circuit element $C_{\rm sc}$, as well as C_t, R_t, and g_m.
3) As the optical input power increases beyond 10 mW, the C_t and R_t values rapidly changes in an inverse fashion to each other, increasing the time constant.
4) The value of $C_{\rm sc}$ also tends to increase as the optical input power level increases due to additional stored charge effects.
5) The best-fitted values of $g_m e_o(0)$, which determines the dc level of the calculated frequency response, increases linearly below 12.6 mW optical input power and gradually saturates beyond this power level.

V. Discussion

By incorporating the new component $C_{\rm sc}$ and corresponding 3-dB bandwidth $f_{C_{\rm sc}}$, the total 3-dB bandwidth of the p-i-n PD can be represented with (7)

$$\frac{1}{f_{3\,\rm dB}^2} = \frac{1}{f_{C_{\rm sc}}^2} + \frac{1}{f_t^2} + \frac{1}{f_{CR}^2} \tag{7}$$

where the carrier-transit-time-limited 3-dB bandwidth f_t corresponds to the 3-dB bandwidth of the C_tR_t circuit $f_{C_tR_t}$. Using the best-fitted values of the time-delay components C_t, R_t, and $C_{\rm sc}$ in Fig. 7, the values of $f_{C_{\rm sc}}$ and f_t can be calculated from (5) and (6), respectively, by setting them equal to -3 dB. Based on the calculation results, some conclusion can be reached as discussed below.

When the optical input power level $(P_{\rm in})$ is below 10 mW (photocurrent: 8.3 mA), the first term in (6) can be ignored. Hence, the measured optical-frequency response can be well fitted by best choosing the time-delay circuit elements C_t, R_t, and g_m.

By increasing the optical input power level $(P_{\rm in})$ over 10 mW, the side-illuminated p-i-n PD exhibits a serious degradation in the frequency response $(f_{3\,\rm dB})$ as the optical input power (photocurrent) increases. This degradation of the responses at high photocurrents is physically related to the formation of the extended regions of the low electric field that are very analogous to the Kirk effect in bipolar transistors [11]. It is well known that a reduced electric field will further reduce the transit velocity of the photo carrier and enlarge the carrier transit-induced time delay. Thus, just as discussed for the above curve-fitting results, this can be represented by an increase of the electrical time constant of the R_tC_t circuit. This explains well that an additional space charge effect is induced in the high power. The values of R_t and C_t varies with the optical input power levels.

In the very high optical input power level case, the value of $f_{C_{\rm sc}}$ is seriously decreased. For example, at an optical input power level $(P_{\rm in})$ of 32 mW, the value of $f_{C_{\rm sc}}$ is decreased to nearly 21 GHz (as shown in Fig. 6). Although the measured bandwidth of the studied WG p-i-n PD $f_{3\,\rm dB}$ is dominated by the 3-dB bandwidth f_t due to carrier-transit-time effect (nearly 2 GHz, as shown in Fig. 6), the effect of $f_{C_{\rm sc}}$ becomes remarkable in the high-frequency region. It was reported that a charge storage within the PD possibly develops a current waveform distortion at sufficiently high frequency in the high-power condition [11]. This is to say that, for a very large input power and output current level, the depletion capacitance could be instantaneously modulated, thus yielding a further nonlinear effect. This is called the stored charge effect. As shown in Fig. 7, the measured optical frequency response curves in the high-frequency region for the high-power case can also be well fitted using the high-power equivalent circuit that was newly proposed by further combining the effect of the parallel circuit element $C_{\rm sc}$. This result proves that the newly added parallel circuit element $C_{\rm sc}$ is considered to represent the additional space charge effect (stored charge effect).

Finally, let us give some discussion on the transconductance g_m that was defined with a VCCS. A linear increase of $g_me_o(0)$, which represents the dc response of the equivalent circuit, was observed in Fig. 9 at optical power levels up to 12.6 mW. Assuming that the $e_o(0)$ of the equivalent circuit increases linearly with the optical input power (photocurrent) level, the linear behavior gives a constant g_m in the studied optical input power range. At higher optical input power levels, a gradual saturation of the best-fitted value of $g_me_o(0)$ was observed. The contribution each of g_m and $e_o(0)$ for the dc current saturation should be further evaluated to establish further an accurate equivalent-circuit model.

VI. Conclusion

In summary, we have proposed a high-power equivalent-circuit model of p-i-n PDs by taking account of both space charge-induced carrier-transit-time delay effect and stored charge effect in the high-power operating condition. Although some physical formulation cannot be reached by this paper, this new model gives a good approximation with the measured optical response of ultrafast high-power WG p-i-n PDs, as well as being well associated with the physical explanation of the high-power behavior of the p-i-n PDs. This approach provides a method that directly predicts and analyses the high-power properties of ultrafast p-i-n PDs using a full electrical equivalent circuit, and will be helpful to design high-speed and high-power p-i-n PDs.

References

[1] G. Wang, T. Tokumitsu, I. Hanawa, K. Sato, and M. Kobayashi, "Analysis of high speed p-i-n photodiodes S-parameters by a novel small-signal equivalent circuit model," *IEEE Microwave Wireless Comp. Lett.*, vol. 12, pp. 378–380, Oct. 2002.

[2] K. Kato, "Ultrawide-band/high-frequency photodetectors," *IEEE Trans. Microwave Theory Tech.*, vol. 47, pp. 1265–1280, July 1999.

[3] Y. L. Huang and C. K. Sun, "Nonlinear saturation behaviors of high-speed p-i-n photodiodes," *J. Lightwave Technol.*, vol. 18, pp. 203–212, Feb. 2000.

[4] G. Lucovsky, R. F. Schwarz, and R. B. Emmons, "Transit-time considerations in p-i-n diodes," *J. Appl. Phys.*, vol. 35, pp. 622–628, 1964.

[5] J. M. Zhang and D. R. Conn, "State-space modeling of the p-i-n photodetectors," *J. Lightwave Technol.*, vol. 10, pp. 603–609, May 1992.

[6] J. J. Liu, C. K. Liu, C. M. Hsiao, H. H. Lin, and H. C. Lee, "Time-delay circuit model of high-speed p-i-n photodiodes," *IEEE Photon. Technol. Lett.*, vol. 14, pp. 525–527, Apr. 2002.

[7] N. Yasuoka, M. Makiuchi, M. Miyata, O. Aoki, M. Egawa, N. Okazaki, M. Takechi, H. Kuwatsuka, and H. Soda, "High-efficiency p-i-n photodiodes with a spot-size converter for 40 Gb/s transmission systems," in *Proc. ECOC*, Sept.–Oct. 30–4, 2001, pp. 558–559.

[8] J. Schlafer, C. B. Su, W. Powazinik, and R. B. Lauer, "20 GHz bandwidth InGaAs photodetectors for long-wavelength microwave optical links," *Electron. Lett.*, vol. 21, pp. 496–471, 1985.

[9] K. Kato, S. Hata, K. Kawano, and A. Kozen, "Design of ultrawide-band, high-sensitivity p-i-n-photodetectors," *IEICE Trans. Electron*, vol. E76-C, pp. 214–221, 1993.

[10] S. Wang, *Fundamentals of Semiconductor Theory and Device Physics.* Englewood Cliffs, NJ: Prentice-Hall, 1986, p. 654.

[11] D. C. Herbert, E. Chidley, M. Allenson, and D. Wight, "A theory for the nonlinear response of high power p-i-n photodetectors," *J. Appl. Phys.*, vol. 48, pp. 634–640, 1998.

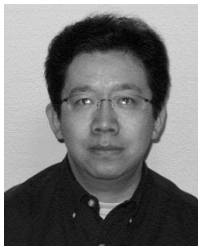

Gang Wang was born in China, in 1968. He received the B.E. degree from Jilin University, Changchun, Jilin Province, China, in 1991, and the M.E. and Ph.D. degrees from Nagoya Institute of Technology, Nagoya, Japan, in 1998, and 2001, respectively.

In 2001, he joined Fujitsu Quantum Devices Limited, Yamanashi, Japan, where he is currently involved with research and development of photodetectors for fiber-optic communication systems. He has authored over 20 professional journal papers.

Tsuneo Tokumitsu (M'88–SM'02) received the B.S. and M.S. degrees from Hiroshima University, Hiroshima, Japan, in 1974 and 1976, respectively, and the Ph.D. degree from Tohoku University, Sendai, Japan, in 1998.

In 1976, he joined the Nippon Telegraph and Telephone Public Corporation (now NTT), Yokosuka, Japan, where he had been involved in developmental research on microwave and millimeter-wave GaAs FET circuits and monolithic microwave integrated circuits (MMICs). In September 1986, he joined ATR Optical and Radio Communication Research Laboratories, Osaka, Japan, while on leave from NTT. While with ATR Optical and Radio Communication Research Laboratories, his primary interests were achieving FET-sized ultra-wide-band circuit function modules (LUFETs), multilayer structures, and active inductors (all for MMICs). In February 1990, he joined NTT Radio Communication Systems Laboratories, Yokosuka, Japan, where he accomplished high-linearity MMIC transmit/receive (T/R) modules for NTT 16-QAM systems in 1993 and a 2-V 1-W T/R switch MMIC in 1994. During these developments, he began developmental research on advanced uniplanar and three-dimensional (3-D)/Masterslice MMIC technologies. In 1999, he joined Fujitsu Quantum Devices Limited, Yamanashi, Japan, where he is currently a Director of the Device Technology Division. He has authored and coauthored 48 transaction and journal papers and 38 international conference papers. He also coauthored a book on MMIC published by the IEICE, Tokyo, Japan.

Dr. Tokumitsu served on the IEEE Microwave and Millimeter-Wave Monolithic Circuit Symposium and RFIC Symposium from 1995 to 2000. He currently serves on the IEEE Microwave Theory and Techniques Society (IEEE MTT-S) International Microwave Symposium. He was a recipient of the 1991 IEEE MTT-S Microwave Prize, the 1994 Ichimura Prize in Technology—Meritorious Achievement presented by the New Technology Development Foundation, and the 1994 Japan Microwave Prize presented at the Asia–Pacific Microwave Conference, Tokyo, Japan.

Ikuo Hanawa was born in Japan, in 1961. He received the M.E. degree from Shinshu University, Ueda City, Nagano Prefecture, Japan, in 1988.

In 1989, he joined Fujitsu Quantum Devices Limited, Yamanashi, Japan, where he has been engaged in the development of InGaAs PDs for fiber-optic communication.

Yoshihiro Yoneda was born in Nara, Japan, in 1970. He received the B.E. and M.E. degrees from the Nagoya Institute of Technology, Nagoya, Japan, in 1994, and 1996, respectively.

In 1996, he joined Fujitsu Laboratories Ltd., Kanagawa, Japan, where he was engaged in research and development of semiconductor lasers, including their packaging technologies. In 1999, he joined Fujitsu Quantum Devices Limited, Yamanashi, Japan, where he is currently involved with the development of photodetectors for fiber-optic communication systems. His interests are opto-electronic devices and opto-electronic integrated circuits/modules.

Mr. Yoneda is a member of the Institute of Electronics, Information and Communication Engineers (IEICE), Japan.

Keiji Sato received the B.S. degree from Tokyo Science University, Tokyo, Japan, in 1986.

In 1986, he joined Fujitsu Ltd. Since 1998, he has been with Fujitsu Quantum Devices Limited, Yamanashi, Japan, where he has been engaged in design and development of photodetectors/receiver modules.

Masahiro Kobayashi received the B.E. and M.E. degrees from the Nagoya Institute of Technology, Nagoya, Japan, in 1981 and 1983, respectively.

In 1983, he joined Fujitsu Laboratories Ltd., Atsugi, Japan. Since 1997, he has been with Fujitsu Quantum Devices Limited, Yamanashi, Japan, where he has been engaged in research and development of compound semiconductor devices and integrated modules for lightwave communication application.

Mr. Kobayashi is a member of the Japan Society of Applied Physics and the Institute of Electronics, Information and Communication Engineering (IEICE), Japan.